

# Cage-like $B_{40}^+$ : a perfect borospherene monocation

Hai-Ru Li<sup>1</sup> · Qiang Chen<sup>1</sup> · Xin-Xin Tian<sup>1</sup> · Hai-Gang Lu<sup>1</sup> · Hua-Jin Zhai<sup>1</sup> · Si-Dian Li<sup>1</sup>

Received: 4 February 2016 / Accepted: 6 April 2016 / Published online: 11 May 2016  
© Springer-Verlag Berlin Heidelberg 2016

**Abstract** The recent discovery of perfect cage-like  $D_{2d} B_{40}^-$  and  $D_{2d} B_{40}$  (all-boron fullerenes) has led to the emergence of a borospherene family. However, the geometrical and electronic structures of their cationic counterpart  $B_{40}^+$ , previously detected in gas phase, remain unknown to date. Based on extensive first-principles theory calculations, we present here in the possibility of a perfect cage-like  $D_{2d} B_{40}^+$  (**1**) ( ${}^2A_1$ ) for the monocation, which turns out to be the global minimum of the system similar to  $B_{40}^-$  and  $B_{40}$ , adding a new member to the borospherene family. Molecular dynamics simulations indicate that  $D_{2d} B_{40}^+$  (**1**) is dynamically stable at 300 K, whereas it starts to fluctuate at 500 K between the two lowest-lying isomers  $D_{2d} B_{40}^+$  (**1**) (**W**) and  $C_s B_{40}^+$  (**3**) (**M**) in concerted **W-X-M** mechanisms via the transition state of  $C_1 B_{40}^+$  (**X**), with forward (**W** → **X** → **M**) and backward (**M** → **X** → **W**) activation energies ( $E_a$ ) of 14.6 and 6.9 kcal mol<sup>-1</sup>, respectively. The spectra from IR, Raman, and UV–vis analyses were simulated to facilitate future characterization of this important borospherene monocation.

**Keywords** Borospherene · Monocation ·  $B_{40}^+$  · First-principles theory · IR · Raman · UV–vis

## Introduction

Boron, a typical electron-deficient element in the periodical table, has a rich chemistry dominated by multicenter-two-electron bonds (mc-2e bonds) in both polyhedral molecules and bulk allotropes [1]. Interestingly, multicenter bonding is also found to be responsible for the formation of planar or quasi-planar structures in a wide range of gas-phase boron clusters  $B_n^{-/0}$  ( $n = 3–25, 27, 30, 35, 36$ ) characterized in recent years by Wang and coworkers [2–13]. In these flat species, neighboring periphery boron atoms are bonded with localized 2c–2e  $\sigma$  bonds along the boundary, while the inner atoms and the periphery atoms are sewn together in blocks with delocalized multicenter  $\sigma$  and  $\pi$  bonds. Furthermore, multicenter bonds become the sole bonding interactions in the newly discovered borospherenes  $D_{2d} B_{40}^{-/0}$  (all-boron fullerenes, [14]): the perfect cage-like  $D_{2d} B_{40}$  possesses a unique  $\sigma + \pi$  double delocalization bonding pattern with all its 120 valence electrons distributed evenly in 48 delocalized 3c–2e  $\sigma$  bonds (one on each  $B_3$  triangle on the cage surface), and 12 delocalized mc-2e  $\pi$  bonds ( $m = 5, 6, \text{ and } 7$ , one over each boron double chain). No localized 2c–2e bonds exist in these borospherenes. Endohedral  $M@B_{40}$  ( $M = \text{Ca, Sr}$ ) and exohedral  $M\&B_{40}$  ( $M = \text{Be, Mg}$ ) were predicted shortly after at density functional theory (DFT) level by Bai et al. [15]. The electronic and IR and Raman spectra of neutral  $B_{40}$  were also computationally simulated by He and Zeng [16] and Chen et al. [17]. The first axially chiral  $C_3 B_{39}^-$  and  $C_2 B_{39}^-$  were characterized experimentally by Chen et al. in 2015 [18], followed by first-principles theory predictions of the charged borospherenes  $C_1 B_{41}^+$ ,  $C_2 B_{42}^{2+}$  [17],  $C_s B_{38}^{2-}$  [19], and  $T_h$

**Electronic supplementary material** The online version of this article (doi:10.1007/s00894-016-2980-6) contains supplementary material, which is available to authorized users.

✉ Si-Dian Li  
lisidian@yahoo.com  
Hai-Gang Lu  
luhg@sxu.edu.cn  
Hua-Jin Zhai  
hj.zhai@sxu.edu.cn

<sup>1</sup> Institute of Molecular Science, Shanxi University, Taiyuan 030006, Shanxi, People's Republic of China

$B_{36}^{4-}$  [20]. These cubic-box-like  $B_n^q$  clusters form a borospherene family ( $n=36-42$ ,  $q=n-40$ ), which are all composed of 12 interwoven double chains (BDCs) with  $n+8$  triangles and six hexagonal or heptagonal faces on the cage surface, analogous to cubane  $C_8H_8$  [14, 15, 17–20]. All these borospherenes follow the general electron counting rule of 12 delocalized  $\pi$  bonds over 12 interwoven BDCs. The possibility of the cage-like  $B_{44}$  with two nonagons was also reported recently by Tai et al. [21]. The latest development in boron clusters is the experimental characterization by Wang et al. [22] of the seashell-like  $C_2 B_{28}^{-/0}$ , which are the smallest borospherenes observed so far. Another major discovery in boron chemistry in 2015 was the syntheses of the atomically thin monolayer borophenes, with or without vacancies on Ag(111) substrate [23, 24], realizing the boron analogs of graphene experimentally.

As the cationic counterparts of  $B_{40}^-$  and  $B_{40}$ ,  $B_{40}^+$  was first detected with mass spectrometry in the gas phase in 1992 [25]. However, there have been no further theoretical or experimental investigations reported on its geometrical and electronic structures to date. In this investigation, based on extensive first-principles theoretical calculations, we predict the possibility of the perfect cage-like  $D_{2d} B_{40}^+$  (1), which turns out to be the global minimum of the monocation similar to  $B_{40}^-$  and  $B_{40}$ . Extensive molecular dynamics (MD) simulations were performed to investigate its dynamic behaviors. The IR, Raman, and UV–VIS spectra of the borospherene monocation were simulated computationally to facilitate future experiments.

## Methods

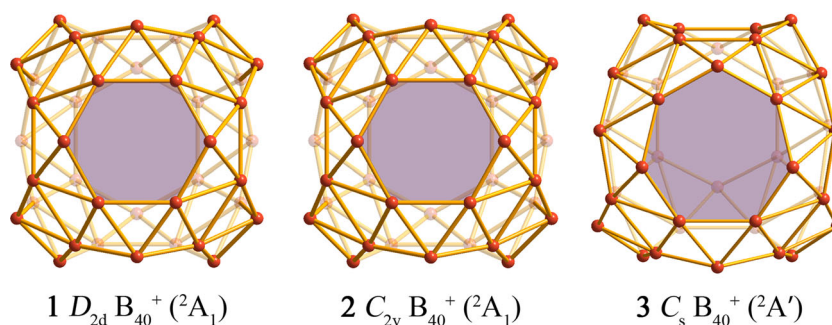
Extensive global-minimum structural searches were performed on  $B_{40}^+$  using the Minima Hopping (MH) approach at DFT level [26, 27], in combination with manual structural constructions based on the low-lying planar, cage-like, and tubular isomers of the observed  $B_{40}^{-/0}$  [14]. Low-lying structures thus obtained were then fully optimized at both the hybridized DFT-PBE0 [28] and DFT-TPSSH [28, 29] levels, with the basis set of 6-311+G(d) [30]. We noted that, although the optimized cage-like  $D_{2d} B_{40}^+$  (1) (see Fig. 1) possesses an imaginary vibrational frequency of  $113.7\text{ cm}^{-1}$  at PBE0 level, it is 0.011 eV more stable than the slightly distorted  $C_{2v} B_{40}^+$  (2) with zero-point corrections included (see Fig. S1 in the Supporting Information). This stability order is strongly supported by the more accurate coupled cluster method CCSD(T) [31–33], which shows that  $D_{2d} B_{40}^+$  (1) lies 0.012 eV lower than  $C_{2v} B_{40}^+$  (2). The two structures are so close in geometry that, with the bond-length criterion of  $0.01\text{ \AA}$ , they are practically the same with the actual symmetry of  $D_{2d}$ . Structural optimizations at DFT-PBE [34, 35], DFT-TPSSH, and DFT-B3PW91 [36, 37] levels further indicate that

$D_{2d} B_{40}^+$  (1) is indeed the lowest-lying isomer of  $B_{40}^+$  without an imaginary frequency, while  $C_{2v} B_{40}^+$  (2) is not even a stationary point on the potential energy surface, which is automatically converted to  $D_{2d} B_{40}^+$  (1) during the optimization processes. We conclude that the imaginary frequency of  $D_{2d} B_{40}^+$  (1) at PBE0 is an artifact of the PBE0 functional.  $D_{2d} B_{40}^+$  (1) is therefore the global minimum (GM) of the monocation, as shown in Fig. S1, where the 20 typical low-lying isomers within 1.55 eV are systematically compared. All calculations in this work were implemented using the Gaussian 09 package [38], whereas the CCSD (T) calculations were achieved using the MOLPRO program [39]. MD simulations were performed for  $B_{40}^+$  (1) at 300 K, 500 K, and 700 K for 30 ps (Fig. S2) using the software suite of CP2K [40]. The UV–vis absorption spectrum of  $D_{2d} B_{40}^+$  (1) was calculated using the time-dependent DFT approach (TD-PBE0) [41] implemented in Gaussian 09.

## Result and discussion

As shown in Figs. 1 and S1,  $B_{40}^+$  possesses a perfect cage-like GM structure with the overall symmetry of  $D_{2d}$  ( $1, ^2A_1$ ), similar to  $D_{2d} B_{40}$ , the GM of the neutral, and  $D_{2d} B_{40}^-$ , the second lowest-lying isomer of the monoanion [14]. Detaching one electron from the highest occupied molecular orbital (HOMO) ( $a_1$ ) of  $D_{2d} B_{40}$  produces only slight bond length changes in the second decimals in  $D_{2d} B_{40}^+$  (1) (within  $0.02\text{ \AA}$ , see Fig. S3). One unpaired  $\alpha$ -electron exists in the undegenerate HOMO-1 ( $a_1$ ) of  $D_{2d} B_{40}^+$  (1), which lies very close in energy with the highest singly occupied  $\alpha$ -molecular orbital ( $\alpha$ -SOMO) ( $a_2$ ) (see Fig. S4). Such an electron detachment produces no structural distortion to the monocation.  $D_{2d} B_{40}^+$  (1) therefore follows both the geometrical and bonding patterns of  $D_{2d} B_{40}$ , with one  $\alpha$ -molecular orbital ( $a_1$ ) singly occupied, similar to  $D_{2d} B_{40}^-$  [14].  $B_{40}^+$  is thus a new member of the borospherene family. Other low-lying isomers are all cage-like or quasi-planar, as collectively depicted in Fig. S1. The cage-like  $C_s B_{40}^+$  (3), which possesses two neighboring hexagons on the top and back, and the cage-like  $C_1 B_{40}^+$  (4), which can be obtained by capping one hexagon on  $C_3 B_{39}^-$  [18] lie 0.34 eV and 0.39 eV higher than the GM at PBE0, respectively. Other quasi-planar (such as 5 and 7) and cage-like (such as 6, 8, 9, and 10) isomers appear to be at least 0.6 eV less stable than the GM at PBE0. The slightly distorted triple-ring tubular  $C_s B_{40}^+$  (20), which can be constructed by capping a B atom on one end of the perfect triple-ring tubular  $B_{39}^-$  [18] appears to be much less stable (by 1.54 eV) than the GM (see Fig. S1). As shown in Fig. S1, the relative energies obtained at TPSSH generally support the PBE0 results, though it slightly favors the quasi-planar  $C_s B_{40}^+$  (5) and  $C_s B_{40}^+$  (7), which possess different curvatures with two adjacent hexagons.

**Fig. 1**  $D_{2d}B_{40}^+$  (1),  $C_{2v}B_{40}^+$  (2), and  $C_s B_{40}^+$  (3) optimized at PBE0/6-311+G(d) level, with the hexagons and heptagons in the front shaded in purple



Extensive MD simulations revealed the dynamic behaviors of the monocation. As shown in Fig. S2,  $D_{2d}B_{40}^+$  (1) is dynamically stable at 300 K, with the root-mean-square-deviation (RMSD)=0.06 Å and the maximum bond length deviation of MAXD=0.19 Å. However, at 500 K (RMSD=0.08 Å, MAXD=0.29 Å), and especially at 700 K (RMSD=0.10 Å, MAXD=0.39 Å), it starts to hop between the two lowest-lying isomers  $D_{2d}B_{40}^+$  (1) (W) and  $C_s B_{40}^+$  (3) (M) in the concerted M-X-M transformation mechanisms proposed recently by Gao et al. [42] for  $B_{39}^-$ , via the transition state of  $C_1 B_{40}^+$  (X), which has one tetracoordinate B atom shared by two neighboring heptagons (Fig. 2). The transition state  $C_1 B_{40}^+$  (X) has an imaginary frequency of 155  $\text{cm}^{-1}$ ; the vibration of the active atom at the center is indicated with an arrow in Fig. 2. The concerted vibrations of the active atom and its close neighbors in the intrinsic reaction coordinates (IRCs) of the system lead to both  $D_{2d}B_{40}^+$  (1) (W) and  $C_s B_{40}^+$  (3) (M), with the forward (W→X→M) and backward (M→X→W) activation energies ( $E_a$ ) of 14.6  $\text{kcal mol}^{-1}$  and 6.9  $\text{kcal mol}^{-1}$ , respectively. With a lower activation energy than  $D_{2d}B_{40}^+$  (1), the second lowest-lying  $C_s B_{40}^+$  (3) is much less populated and shorter lived than the GM, as

shown in Fig. S2 at both 500 K and 700 K. The open-shell  $D_{2d}B_{40}^+$  (1) is obviously less stable dynamically than the closed-shell  $D_{2d}B_{40}$ , which appears to be stable at 1000 K [14] and starts to fluctuate between its lowest-lying isomers at 1200 K [43].

Combining infrared photodissociation (IR-PD) spectroscopy and first-principles calculations has proven to be an effective approach in the characterization of novel cluster monocations [44].  $B_{40}^+$  was previously detected in gas-phase with mass spectrometry [25]. It is therefore possible to measure its IR spectra and characterize its geometrical and electronic structures in experiments under suitable conditions. We simulated the IR spectrum of  $D_{2d}B_{40}^+$  (1) at PBE0 in Fig. 3a to facilitate such measurements. The IR active modes of  $D_{2d}B_{40}^+$  (1) possess the irreducible representations of  $b_2$  and  $e$ , with most of them being weak in IR intensities. The strongest IR vibration occurs at  $\nu_{95}=1104 \text{ cm}^{-1}$  ( $b_2$ ), which exhibits an obvious red-shift with respect to the strongest IR peak of 1274  $\text{cm}^{-1}$  ( $e$ ) calculated for  $D_{2d}B_{40}$  at the same theoretical level [17]. The second, third, and fourth strongest IR peaks are predicted at 528  $\text{cm}^{-1}$  ( $b_2$ ), 490  $\text{cm}^{-1}$  ( $b_2$ ), and

**Fig. 2** Intrinsic reaction coordinates (IRC) of  $B_{40}^+$  from the reactant  $D_{2d}B_{40}^+$  (W), via transition state  $C_1 B_{40}^+$  (X), to product  $C_s B_{40}^+$  (M), with the activation energies indicated in  $\text{kcal mol}^{-1}$  at PBE0/6-311G. The vibrations of the active atom at the center in W, X, and M are indicated with arrows to guide the viewer

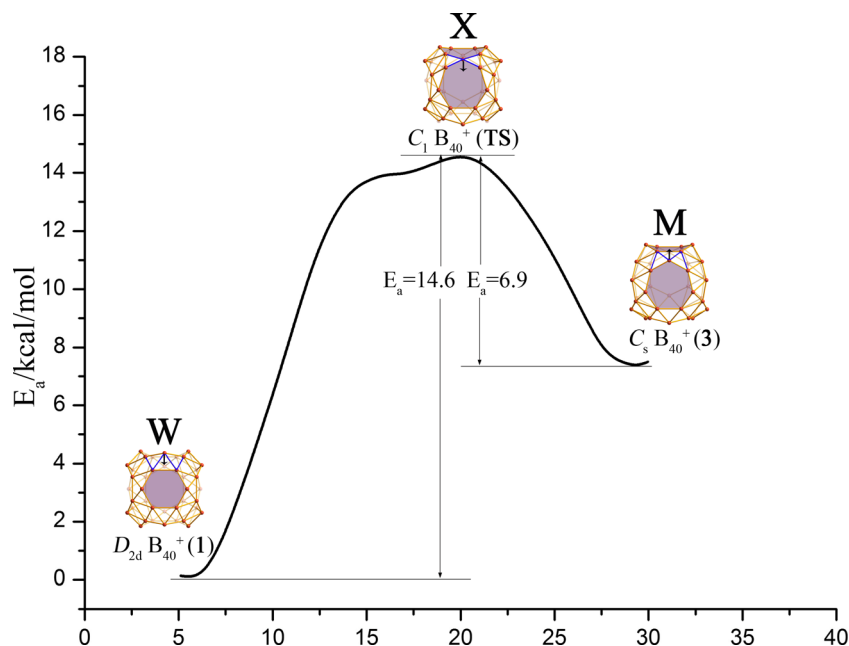
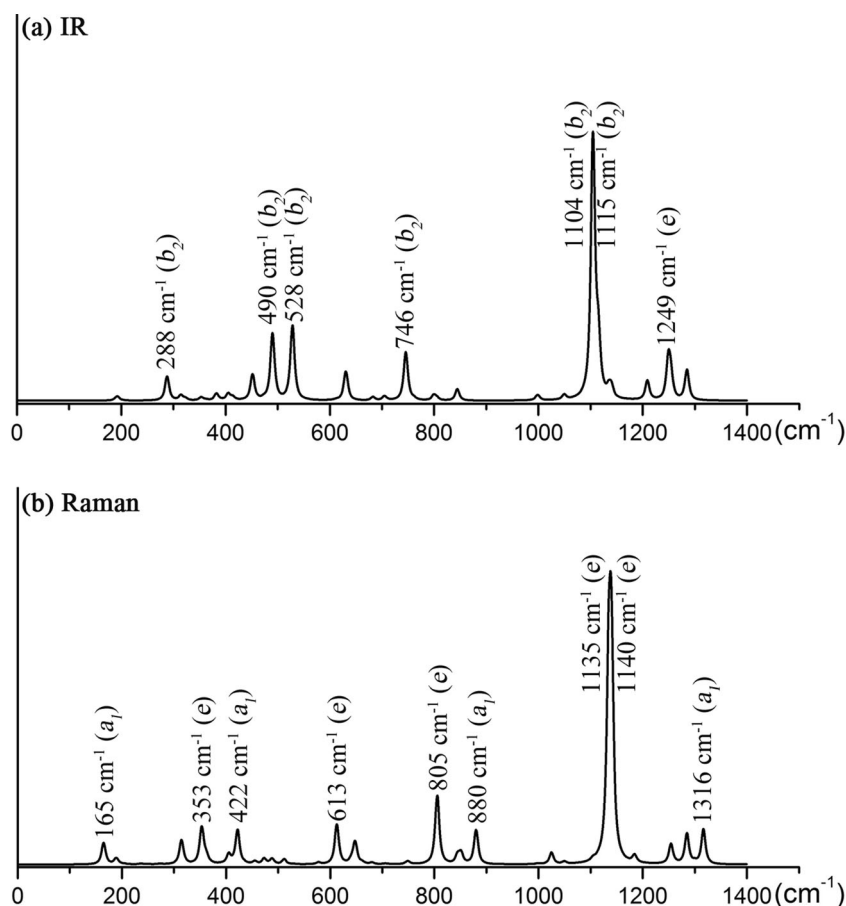


**Fig. 3** Simulated **a** IR and **b** Raman spectra of  $D_{2d}B_{40}^+$  (**1**) at PBE0/6-311+G(d) level



1249  $\text{cm}^{-1}$  ( $e$ ), respectively. These calculated frequencies may serve as fingerprints to characterize  $D_{2d}B_{40}^+$  (**1**) in IR measurements.

The Raman active vibrational modes of  $D_{2d}B_{40}^+$  (**1**) generate irreducible representations of  $e$  and  $a_1$  (Fig. 3b). The strongest Raman scattering peaks of  $D_{2d}B_{40}^+$  (**1**) at  $\nu_{99}=1135 \text{ cm}^{-1}$  ( $e$ ) and  $\nu_{100}=1140 \text{ cm}^{-1}$  ( $e$ ) also exhibit an obvious red-shift (about  $200 \text{ cm}^{-1}$ ) with respect to that of  $D_{2d}B_{40}$  predicted at  $1327 \text{ cm}^{-1}$  ( $a_1$ ) [17]. Among the weak Raman peaks calculated at  $165 \text{ cm}^{-1}$  ( $a_1$ ),  $353 \text{ cm}^{-1}$  ( $e$ ),  $422 \text{ cm}^{-1}$  ( $a_1$ ),  $805 \text{ cm}^{-1}$  ( $e$ ),  $613 \text{ cm}^{-1}$  ( $e$ ), and  $1316 \text{ cm}^{-1}$  ( $a_1$ ), the two  $a_1$  vibrational modes at  $165 \text{ cm}^{-1}$  and  $422 \text{ cm}^{-1}$  belong to typical radial breathing modes (RBMs). RBMs have been used to characterize hollow structures in single-walled boron nanotubes [45].

Finally, we present the simulated UV-vis absorption spectrum of  $D_{2d}B_{40}^+$  (**1**) (Fig. 4), which turns out to have similar spectroscopic features to that of  $D_{2d}B_{40}$  [16], with strong absorption bands located at 215 nm, 234 nm, 273 nm, 314 nm, 377 nm, and 447 nm, respectively. They all involve one-electron excitations from deep inner-shells to high-lying unoccupied orbitals of the monocation. We note that both the excitations from the  $\alpha$ -SOMO to  $\alpha$ -LUMO at 2.13 eV (582 nm), and from  $\beta$ -SOMO to  $\beta$ -LUMO at 0.21 eV (5776 nm), are optically inactive with the oscillator strengths

of zero, in contrast to the weak HOMO-LUMO excitation of  $D_{2d}B_{40}$  at 2.33 eV (532 nm), which is optically active with a small oscillator strength [16].

## Conclusions

We have presented in this work a comprehensive theoretical investigation on the perfect borospherene  $D_{2d}B_{40}^+$  (**1**), which

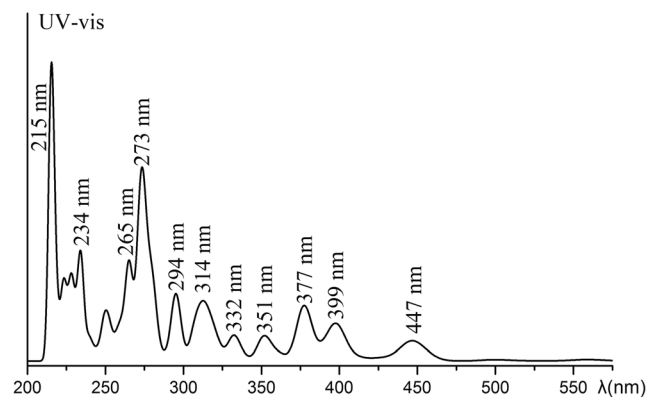


**Fig. 4** Simulated UV-vis absorption spectrum of  $D_{2d}B_{40}^+$  (**1**) at PBE0/6-311+G(d)

turns out to be the GM of the system similar to  $D_{2d} B_{40}^-$  and  $D_{2d} B_{40}$ . MD simulations show that  $D_{2d} B_{40}^+$  (**1**) starts to fluctuate between  $D_{2d} B_{40}^+$  (**1**) and  $C_s B_{40}^+$  (**3**) at 500 K in concerted **W-X-M** mechanisms, similar to the dynamic properties of  $B_{39}^-$  [42],  $B_{40}$  [14, 43],  $B_{41}^+$  and  $B_{42}^{2+}$  [17]. The simulated IR, Raman, and UV–vis spectra of  $D_{2d} B_{40}^+$  (**1**) may facilitate future characterization of this cage-like mono-cation to enrich the chemistry of borospherenes.

**Acknowledgment** This work was supported financially by the National Natural Science Foundation of China (21373130, 21573138, and 21473106).

## References

- Cotton FA, Wilkinson G, Murillo CA, Bochmann M (1999) Advanced inorganic chemistry, 6th edn. Wiley, New York
- Zhai HJ, Alexandrova AN, Birch KA, Boldyrev AI, Wang LS (2003) Hepta- and octacoordinated boron in molecular wheels of eight- and nine-atom boron clusters: observation and confirmation. *Angew Chem Int Ed* 42:6004–6008
- Zhai HJ, Kiran B, Li J, Wang LS (2003) Hydrocarbon analogues of boron clusters—planarity, aromaticity and antiaromaticity. *Nat Mater* 2:827–833
- Kiran B, Bulusu S, Zhai HJ, Yoo S, Zeng XC, Wang LS (2005) From the cover: planar-to-tubular structural transition in boron clusters:  $B_{20}$  as the embryo of single-walled boron nanotubes. *Proc Natl Acad Sci USA* 102:961–964
- Huang W, Sergeeva AP, Zhai HJ, Averkiev BB, Wang LS, Boldyrev AI (2010) A concentric planar doubly  $\pi$ -aromatic  $B_{19}^-$  cluster. *Nat Chem* 2:202–206
- Oger E, Crawford NRM, Kelting R, Weis P, Kappes MM, Ahlrichs R (2007) Boron cluster cation: transition from planar to cylindrical structures. *Angew Chem Int Ed* 46:8503–8506
- Li WL, Zhao YF, Hu HS, Li J, Wang LS (2014)  $[B_{30}]^-$ : a quasiplanar chiral boron cluster. *Angew Chem Int Ed* 53:5540–5545
- Li WL, Chen Q, Tian WJ, Bai H, Zhao YF, Hu HS, Li J, Zhai HJ, Li SD, Wang LS (2014) The  $B_{35}$  cluster with a double-hexagonal vacancy: a new and more flexible structural motif for borophene. *J Am Chem Soc* 136:12257–12260
- Piazza ZA, Hu HS, Li WL, Zhao YF, Li J, Wang LS (2014) Planar hexagonal  $B_{36}$  as a potential basis for extended single-atom layer boron sheets. *Nat Commun* 5:3113(6)
- Chen Q, Wei GF, Tian WJ, Bai H, Liu ZP, Zhai HJ, Li SD (2014) Quasi-planar aromatic  $B_{36}$  and  $B_{36}^-$  clusters: all-boron analogues of coronene. *Phys Chem Chem Phys* 16:18282–18287
- Alexandrova AN, Boldyrev AI, Zhai HJ, Wang LS (2006) All-boron aromatic clusters as potential new inorganic ligands and building blocks in chemistry. *Coord Chem Rev* 250:2811–2866
- Romanescu C, Galeev TR, Li WL, Boldyrev AI, Wang LS (2013) Transition-Metal-Centered monocyclic boron wheel clusters ( $M\odot B_n$ ): a new class of aromatic borometallic compounds. *Acc Chem Res* 46:350–358
- Sergeeva AP, Popov IA, Piazza ZA, Li WL, Romanescu C, Wang LS, Boldyrev AI (2014) Understanding boron through size-selected clusters: structure, chemical bonding, and fluxionality. *Acc Chem Res* 47:1349–1358
- Zhai HJ, Zhao YF, Li WL, Chen Q, Bai H, Hu HS, Piazza ZA, Tian WJ, Lu HG, Wu YB, Mu YW, Wei GF, Liu ZP, Li J, Li SD, Wang LS (2014) Observation of an all-boron fullerene. *Nat Chem* 6:727–731
- Bai H, Chen Q, Zhai HJ, Li SD (2015) Endohedral and exohedral metalloborospherenes:  $M@B_{40}$  ( $M = Ca, Sr$ ) and  $M\&B_{40}$  ( $M = Be, Mg$ ). *Angew Chem Int Ed* 54:941–945
- He RX, Zeng XC (2015) Electronic structures and electronic spectra of all-boron fullerene  $B_{40}$ . *Chem Commun* 51:3185–3188
- Chen Q, Zhang SY, Bai H, Tian WJ, Gao T, Li HR, Miao CQ, Mu YW, Lu HG, Zhai HJ, Li SD (2015) Cage-like  $B_{41}^+$  and  $B_{42}^{2+}$ : new chiral members of the borospherene family. *Angew Chem Int Ed* 54:8160–8164
- Chen Q, Li WL, Zhao YF, Zhang SY, Hu HS, Bai H, Li HR, Tian WJ, Lu HG, Zhai HJ, Li SD, Wang LS (2015) Experimental and theoretical evidence of an axially chiral borospherene. *ACS Nano* 9:754–760
- Chen Q, Li HR, Miao CQ, Wang YJ, Lu HG, Mu YW, Ren GM, Zhai HJ, Li SD (2016) Endohedral  $Ca@B_{38}$ : stabilization of a  $B_{38}^{2-}$  borospherene dianion by metal encapsulation. *Phys Chem Chem Phys*. doi:10.1039/c5cp06169e
- Tian WJ, Chen Q, Li HR, Yan M, Mu YW, Lu HG, Zhai HJ, Li SD (2016) Saturn-like charge-transfer complexes  $Li_4\&B_{36}$ ,  $Li_5\&B_{36}^+$ , and  $Li_6\&B_{36}^{2+}$ : exohedral metalloborospherenes with a perfect cage-like  $B_{36}^{4-}$  core. *Phys Chem Chem Phys*. doi:10.1039/C6CP01279E
- Tai TB, Nguyen MT (2016) A new chiral boron cluster  $B_{44}$  containing nonagonal holes. *Chem Commun* 52:1653–1656
- Wang YJ, Zhao YF, Li WL, Jian T, Chen Q, You XR, Ou T, Zhao XY, Zhai HJ, Li SD, Li J, Wang LS (2016) Observation and characterization of the smallest borospherene,  $B_{28}^-$  and  $B_{28}$ . *J Chem Phys* 144:064307
- Mannix AJ, Zhou XF, Kiraly B, Wood JD, Alducin D, Myers BD, Liu XL, Fisher BL, Santiago U, Guest JR, Yacaman MJ, Ponce A, Oganov AR, Hersam MC, Guisinger NP (2015) Synthesis of borophenes: anisotropic, two-dimensional boron polymorphs. *Science* 350:1513–1516
- Feng BJ, Zhang J, Zhong Q, Li WB, Li S, Li H, Cheng P, Meng S, Chen L, Wu KH (2016) Experimental realization of two-dimensional boron sheets. *Arxiv*:1512.05029
- Placa SJL, Roland PA, Wynne JJ (1992) Boron clusters ( $B_n$ ,  $n = 2-52$ ) produced by laser ablation of hexagonal boron nitride. *Chem Phys Lett* 190:163–168
- De S, Willand A, Amsler M, Pochet P, Genovese L, Goedecker S (2011) Energy landscape of fullerene materials: a comparison of boron to boron nitride and carbon. *Phys Rev Lett* 106:225502
- Goedecker S, Hellmann W, Lenosky T (2005) Global minimum determination of the Born-Oppenheimer surface within density functional theory. *Phys Rev Lett* 95:055501
- Adamo C, Barone V (1999) Toward reliable density functional methods without adjustable parameters: the PBE0 model. *J Chem Phys* 110:6158–6170
- Tao JM, Perdew JP, Staroverov VN, Scuseria GE (2003) Climbing the density functional ladder: nonempirical meta-generalized gradient approximation designed for molecules and solids. *Phys Rev Lett* 91:146401
- Krishnan R, Binkley JS, Seeger R, Pople JA (1980) Self-consistent molecular orbital methods. XX. A basis set for correlated wavefunctions. *J Chem Phys* 72:650–654
- Čížek J (1969) On the use of the cluster expansion and the technique of diagrams in calculations of correlation effects in atoms and molecules. *Adv Chem Phys* 14:35–89
- Purvis GD III, Bartlett RJ (1982) A full coupled-cluster singles and doubles model: the inclusion of disconnected triples. *J Chem Phys* 76:1910–1918
- Raghavachari K, Trucks GW, Pople JA, Head-Gordon M (1989) A fifth-order perturbation comparison of electron correlation theories. *Chem Phys Lett* 157:479–483

34. Perdew JP, Burke K, Ernzerhof M (1996) Generalized gradient approximation made simple. *Phys Rev Lett* 77:3865–3868
35. Perdew JP, Burke K, Ernzerhof M (1997) Errata: Generalized gradient approximation made simple. *Phys Rev Lett* 78:1396
36. Becke AD (1993) Density-functional thermochemistry. III. The role of exact exchange. *J Chem Phys* 98:5648–5652
37. Perdew JP, Ziesche EP, Eschrig H (1991) *Electronic Structure of Solids '91*. Akademie, Berlin
38. Frisch MJ, Trucks GW, Schlegel HB, Scuseria GE, Robb MA, Cheeseman JR, Scalmani G, Barone V, Mennucci B, Petersson GA et al (2013) Gaussian 09, revision D.01. Gaussian, Inc, Wallingford
39. Werner HJ, Knowles PJ, Knizia G, Manby FR, Schütz M, Celani P, Korona T, Lindh R, Mitrushenkov A, Rauhut G, et al (2012) MOLPRO, version 2012.1.
40. VandeVondele J, Krack M, Mohamed F, Parrinello M, Chassaing T, Hutter J (2005) Quickstep: fast and accurate density functional calculations using a mixed Gaussian and plane waves approach. *Comput Phys Commun* 167:103–128
41. Bauernschmitt R, Ahlrichs R (1996) Treatment of electronic excitations within the adiabatic approximation of time dependent density functional theory. *Chem Phys Lett* 256:454–464
42. Gao TT, Chen Q, Mu YW, Lu HG, Li SD (2016) “W-X-M” transformation in isomerization of B<sub>39</sub><sup>-</sup> borospherenes. *J Chem Phys* (in press)
43. Martínez-Guajardo G, Cabellos JL, Díaz-Celaya A, Pan S, Islas R, Chattaraj PK, Heine T, Merino G (2015) Dynamical behavior of borospherene: a nanobubble. *Sci Rep* 5:11287. doi:[10.1038/srep11287](https://doi.org/10.1038/srep11287)
44. Wang GJ, Zhou MF, Goettel JT, Schrobilgen GJ, Su J, Li J, Schlöder T, Riedel S (2014) Identification of an iridium-containing compound with a formal oxidation state of IX. *Nature* 514:475–477
45. Ciuparu D, Klie RF, Zhu YM, Pfefferle L (2004) Synthesis of pure boron single-wall nanotubes. *J Phys Chem B* 108:3967–3969